

Wavelet Analysis of High-Speed Transition and Turbulence over a Flat Surface

George Khujadze,^{1, a)} Dimitris Drikakis,^{2, b)} Konstantinos Ritos,^{3, c)} Ioannis W. Kokkinakis,^{2, d)} and S. Michael Spottswood⁴

¹⁾University of Siegen, 57068 Siegen, Germany

²⁾University of Nicosia, Nicosia, CY-2417, Cyprus

³⁾University of Thessaly, Volos 38221, Greece

⁴⁾Air Force Research Laboratory, Wright Patterson AFB, Ohio 45433-7402, USA

This paper presents a study of high speed boundary layers using the wavelet method. We analyse direct numerical simulation data for high-speed, compressible transitional and turbulent boundary layer flows using orthogonal anisotropic wavelets. The wavelet-based method of extraction of coherent structures is applied to the flow vorticity field, decomposed into coherent and incoherent contributions using thresholding of the wavelet coefficients. We show that the coherent part of the flow, enstrophy spectra, are close to the statistics of the total flow, and the energy of the incoherent, noise-like background flow is equidistributed. Furthermore, we investigate the distribution of the incoherent vorticity in the transition and turbulent regions and examine the correlation with the near-wall pressure fluctuations. The results of our analysis suggest that the incoherent vorticity part is not a random 'noise' and correlates to the actual noise emanating from inside the boundary layer. This could have implications regarding our understanding of the physics of compressible boundary layers and the development of engineering models.

I. INTRODUCTION

The study is motivated by advancing the understanding of the physics of transitional and turbulent boundary layers (BL) and the relationship of different flow parameters. In particular, the study concerns the high-speed regime (Mach 6), the role of incoherent vorticity and its relationship with pressure fluctuations. The latter is responsible for the noise generated inside the boundary layer and has implications in the acoustic vibrations and, subsequently, acoustic fatigue. These issues are exaggerated in extreme flow environments such as supersonic and hypersonic boundary flows.

Several experimental and numerical studies of high-speed, turbulent boundary layers have been published¹⁻¹². The above studies provide data that advance understanding of the flow processes and guide the design of engineering models. Furthermore, direct numerical simulations have shown that the transition process in hypersonic boundary layers is highly random due to higher modes' existence. The random nature of the hypersonic transition process explains its sensitivity to changes in the disturbance environment that can significantly change the transition process⁷. Most of the studies focused on single-mode or 'controlled' transition, but more recent studies considered multimode perturbations, which comprise many waves imitating the von Kármán atmospheric turbulence^{8,9,13}.

Resolving all dynamically active flow scales requires a high-resolution close to the wall. Other mathematical tools complementary to DNS could also provide significant insight into complex flow physics. It is well-known that turbulent

flows are characterized by a range of spatial and temporal scales, which involves many degrees of freedom interacting nonlinearly. The coherent structures in time and space are observed even at large Reynolds numbers and a random background flow. The computational challenge is that scales increase drastically with Reynolds number. Therefore, detecting and tracking energy-containing eddies to describe turbulent flows with minimum degrees of freedom is essential for studying fluid and acoustics dynamic processes.

Wavelets offer a framework for analyzing turbulent flows based on the ability of wavelet multiresolution analysis to identify and isolate the energetic coherent structures that govern the dynamics of the flow¹⁴. Wavelets are well-defined and -localised in space and scale, and can be efficiently used for multiscale decomposition¹⁴⁻²¹. The wavelet decomposition of turbulent flows concentrates the most energetic coherent structures in a few wavelet coefficients, while the incoherent background flow is represented with the large majority of the wavelet coefficients that keep a negligibly small intensity.

One of the developed methods is the coherent vortex extraction (CVE) from turbulent flow¹⁶, which we present in the next section. CVE is related to denoising signals in wavelet space. Its main idea is to decompose the flow into coherent (represented by a few wavelet coefficients) and incoherent parts (noise) using wavelet filtering of the vorticity field. The evolution of the coherent part of the flow is computed deterministically, whereas the influence of the incoherent background flow is modeled statistically. No model is needed for coherent structures definition. Instead, the noise should be modeled more trivial and is assumed to be additive, Gaussian and white. The general properties of CVE were discussed in the literature^{14,15}. Wavelets are basis functions localized in both physical and wave-number spaces. For comparison, the classical Fourier transform is based on well-localized functions in wave-number space. Still, it does not provide localization in physical space, leading to the lack of general theory in the latter. The previous studies show that CVE

^{a)}Electronic mail: georgekh@yahoo.com, george.khujadze@uni-siegen.de

^{b)}Electronic mail: Author to whom correspondence should be addressed: drikakis.d@unic.ac.cy. Also at the University of Nicosia Research Foundation.

^{c)}Electronic mail: konritos@uth.gr

^{d)}Electronic mail: kokkinakis.i@unic.ac.cy

can more efficiently extract the coherent structures than the Fourier filtering^{14–19,21}.

For wall-bounded flows, the situation becomes more complex because no-slip boundary conditions have to be considered. Indeed, no-slip boundary conditions generate vorticity due to the viscous flow interactions with the walls. In the paper by Khujadze *et al.*²⁰, an efficient algorithm to extract coherent vorticity was developed. A locally refined grid was constructed using wavelets for incompressible turbulent boundary layers with mirror boundary conditions. It was shown that less than 1% of wavelet coefficients retain the coherent structures of the flow, while the majority of the coefficients correspond to a structureless, noise-like background flow. Furthermore, scale- and direction-dependent statistics in wavelet space quantify the flow properties at different wall distances.

This study uses wavelets to analyze recently-published, high-fidelity data from transitional and turbulent BL at Mach 6¹³. We present the coherent and incoherent parts of the flow and enstrophy spectra across the transition and turbulent regions. Furthermore, we discuss the distributions of the incoherent vorticity component and identify a correlation with the near-wall pressure fluctuations. The results of this study prompt further exploration of the relationship between incoherent vorticity and near-wall noise, which could advance understanding of high-speed, near-wall transition and turbulence and guide the development of engineering models.

II. HIGH-RESOLUTION FLOW DATA

The data used in the present study were obtained from the Direct Numerical Simulations (DNS) of Drikakis *et al.*¹³ They concern a hypersonic flow over a flat plate at Mach 6, subjected to von Kármán atmospheric perturbations at the inlet, with a turbulence intensity of the freestream velocity equal to 1%. A detailed description of the method used in the DNS can be found in the study by Kokkinakis *et al.*²² and the flow parameters in the paper by Drikakis *et al.*¹³. A reference length of $x_l = 2$ mm, calculated as the distance from the leading edge of the plate, has been used to non-dimensionalize the data. The Reynolds number is $Re_{x_l} = 77,791$. Similar to previous boundary layer studies in the Mach number range 4 to 6^{10,12,23–27}, the vibrational excitation and dissociation effects of diatomic molecules that could lead to ionization, are neglected. This is further justified as the maximum temperature experienced by the fluid is well below the critical temperature for oxygen dissociation (2500 K).

The DNS solved the full Navier-Stokes equations using a finite volume Godunov-type method in conjunction with the 9th-order Weighted-Essentially-Non-Oscillatory (WENO)²². The computational grid comprised of $4055 \times 405 \times 605$ cells, i.e., 989.2 million cells in total. The grid resolution gave $\Delta x^+ = 2.25$, $\Delta y_w^+ = 0.16$, and $\Delta z^+ = 0.90$, thus we expect that the boundary layer is adequately resolved. Furthermore, the maximum y^+ value at the edge of the boundary layer was $\Delta y_e^+ = 1.89$, providing extra confidence in the accuracy of the results. The DNS aimed to capture the smallest possible tur-

bulent scales and their associated acoustic loading near-wall effects. The simulations had captured both transition and fully turbulent flow regions, and further details on the results and flow physics analysis can be found in the reference study of Drikakis *et al.*¹³.

III. COHERENT VORTICITY EXTRACTION (CVE) USING ORTHOGONAL WAVELETS

In this section, an outline of CVE method is given. The underlying idea is to perform denoising of vorticity field, $\boldsymbol{\omega}(\mathbf{x}) = \nabla \times \mathbf{V}$, in the wavelet coefficient space. We have used Morkovin's hypothesis²⁸ to assess the applicability of the wavelet method near the wall as it does not account for compressibility effects. We found that the root-mean-square fluctuations of the density near the plate are small (maximum value around 0.07). Therefore, according to Morkovin's hypothesis - see also Bradshaw²⁹ and cite Shyy and Krishnamurty³⁰ - the above level of density fluctuations (i.e., less than 0.1) implies that the structure of turbulence (at least near the wall) is "about the same" as that of incompressible flows. Thus, we have employed the present wavelet method based on the above conclusion. We believe that compressibility and dilatational effects deserve further investigation beyond the scope of this paper. The vorticity field is given on a grid (x_i, y_j, z_k) for $i, j, k = 0, N-1$ with $N = 2^{3J}$. J is the corresponding number of octaves, defining the scales from the largest, $l_{max} = 2^0$, to the smallest one, $l_{min} = 2^{1-J}$. The details about the wavelets method can be found in the following publications^{14,15,18,21,31,32}.

The wavelet coefficients threshold is performed with the optimal parameter ε to determine which coefficients belong to the coherent and the incoherent contributions. The latter is assumed to be Gaussian white noise. The threshold parameter ε depends only on the total enstrophy $Z = \frac{1}{2}(\boldsymbol{\omega} \cdot \boldsymbol{\omega})_{xyz}$ and the total number of grid points N as follows: $\varepsilon = \sqrt{4Z \ln N}$ (the choice of ε is based on Donoho's theorem³³). Note that ε has no adjustable parameters. First, using Fast Wavelet Transform (FWT), we compute $\Omega = \sqrt{\sum_{\ell=1}^3 (\overline{\omega_{j_i, k, \ell}^{\mu}})^2}$, where $\omega_{j_i, k, \ell}^{\mu}$ are wavelet coefficients of vorticity. Then, we reconstruct the coherent vorticity $\boldsymbol{\omega}_c$ from those wavelet coefficients for which $\Omega > \varepsilon$. The incoherent vorticity $\boldsymbol{\omega}_i$ is obtained from the remaining weak wavelet coefficients. In the first iteration, the thresholding parameter is defined from ε . Subsequently, a new threshold is determined using the incoherent enstrophy computed from the weak wavelet coefficients instead of the total enstrophy. Then, the thresholding is applied once again, and improved estimators of the coherent and incoherent vorticities are obtained¹⁶. Due to the decomposition's orthogonality, the enstrophy and the threshold can be directly computed in coefficient space using the Parseval's relation. At the end of the iterative procedure, we obtain the coherent and incoherent vorticities reconstructed by Inverse Wavelet Transform (IWT) in the physical space. Finally, we obtain $\boldsymbol{\omega} = \boldsymbol{\omega}_c + \boldsymbol{\omega}_i$ and, by construction, we also have $Z = Z_c + Z_i$. The procedure is schematically presented in Figure 1. The

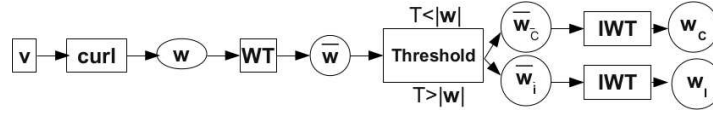
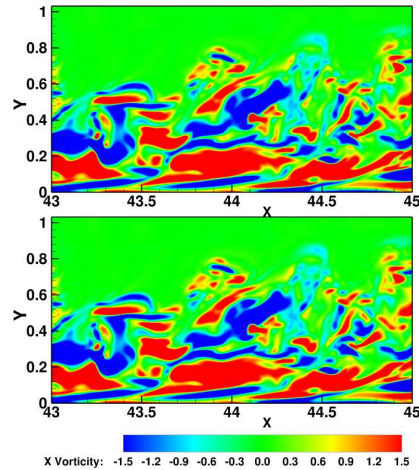


FIG. 1. Schematic presentation of the principles of coherent vorticity extraction.

wavelet method of coherent vorticity extraction proposes a minimal hypothesis: *Coherent structures are not noise*. Thus, removing the noise from the flow field leads to extraction of coherent structures.

The orthogonal wavelet decomposition requires that the number of computational grid points in each coordinate direction is a power of 2. Therefore, the nonuniform grid in the wall-normal direction was interpolated on the uniform one, and the results are shown in Figure 2. The top plot presents the original ω_x field, while the bottom one corresponds to the same field, but interpolated on a uniform grid.

FIG. 2. Slices of ω_x of the original and interpolated data are presented on the top and bottom plots, respectively.

Based on the calculation of the shape factor H , skin friction C_f and Stanton number St on the plate (see Figure 5 in¹³), we split the domain into three regions: the laminar region up to $x = 11.5$ (dimensionless); the transition region $x \in 11.5 - 36.2$ (dimensionless) corresponding to the sudden rise of C_f and St values, and the sudden drop of H ; the fully turbulent region $x \in 36.2 - 50.0$.

The entire transitional region was divided into five different domains to study the statistical characteristics of the flow (Table I). In the region $x \in 11.5 - 16.5$ the energy contained in the incoherent part of the vorticity is 0.001 of total energy for a number of wavelet coefficient exceeding 99% of total number of coefficients. A few wavelet coefficients contain almost the entire enstrophy of the flow.

N	Length	ϵ	Coeff _{coh} (%)	Coeff _{inc} (%)	Energy _{inc}
1	11.5 – 16.5	0.600	0.89	99.10	0.001
2	16.5 – 21.4	1.150	1.42	98.57	0.004
3	21.4 – 26.3	1.619	1.85	98.14	0.012
4	26.3 – 31.3	1.941	2.18	97.82	0.023
5	31.3 – 36.2	1.940	2.25	97.75	0.027
6	36.2 – 50	2.698	2.55	97.75	0.065

TABLE I. Statistics of the vorticity fields in the transition (segments $N = 1 - 5$) and the turbulent region (segment $N = 6$).

Examining the different segments of the transition region, we observe the energy contained by the incoherent part increases while the wavelet coefficients that are necessary to reconstruct them decrease. The wavelet coefficients corresponding to the coherent part of vorticity increase from 0.089% to 2.55% in the fully developed region of the flow. Thus, only about 3% of wavelet coefficients are required to reconstruct the coherent field, which retains more than 99% of the total energy. The rest of the coefficients correspond to the incoherent part. The incoherent part of vorticity is structureless and quasi-homogeneous with low amplitude. Although the remaining majority of wavelet coefficients represent the incoherent flow, they retain a negligible amount of energy compared to the total energy.

Figure 3 shows the results of CVE in the transition region segment 11.5 – 16.5 (dimensionless). The entire field and the coherent and incoherent components are presented using the vorticity magnitude. Since the incoherent part is much weaker than the total and coherent components, its iso-surface values are 25 times smaller than the other two. For comparison, the results of the wavelet decomposition of the transitional region further downstream ($x \in 16.5 - 21.4$) are shown in Figure 4. The energy in this region is a little higher for the incoherent part of vorticity than for the area upstream. Thus, for presentation purposes, we increased the values of the incoherent field by a factor of two. In this case, it looks less organized and structureless than the field in $x \in 11.5 - 16.5$ region.

In Figure 5 the wavelet analysis of the fully developed turbulent region ($x \in 42.6 - 50$) is presented. The values of vorticity magnitude shown on these plots are $|\omega|_{coh} = 5.0$ and $|\omega|_{inc} = 0.5$ for the coherent and incoherent fields, respectively. The statistical parameters for the turbulent region are given in Table I. It is worth noting that the statistics of the transitional regions 4 and 5 are in the range of the statistical parameters of the turbulent region. The largest part of wavelet coefficients represents the incoherent part of the flow, which retains a negligible amount of energy 0.065% of the total energy.

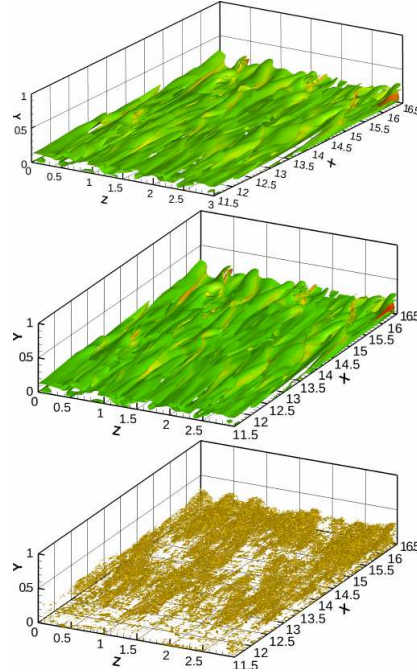


FIG. 3. Total, coherent and incoherent parts of vorticity fields ($|\omega|$) for the transition region $x \in 11.5 - 16.5$ are presented (from top to bottom). Iso-values for total and coherent parts are: $|\omega|_{coh} = 5.0$, for incoherent part $|\omega|_{inc} = 0.2$.

The mean vorticity profiles $\bar{\omega}_z$ against the wall-normal coordinate are shown in figure 6. The spanwise component of the coherent and incoherent components and the total value are averaged in spanwise and streamwise directions. The coherent part preserves the mean profile of spanwise vorticity, while the incoherent component is negligible. Furthermore, we have averaged the incoherent vorticity in the spanwise and streamwise directions (figure 7). Only very close to the wall, the spanwise component differs from zero with minimal amplitude (figure 7), while the other two components are zero.

In figures 8 and 9, the probability density functions (PDF) are presented for the transitional and turbulent regions. In all cases, the PDFs of the total and coherent parts are perfectly superimposed, implying that the high order statistics are well preserved by coherent part. Furthermore, we observe that the vorticity PDFs of the coherent part is skewed in all directions. In contrast, the PDFs of the incoherent parts are symmetric, with significantly reduced variances than the total and coherent PDFs. The above result is similar to the findings of Sakurai et al.²¹ who investigated the PDFs of vorticity for channel flows. They found the coherent component's PDF to be significantly skewed. Here, we observe that the PDF of ω_z is

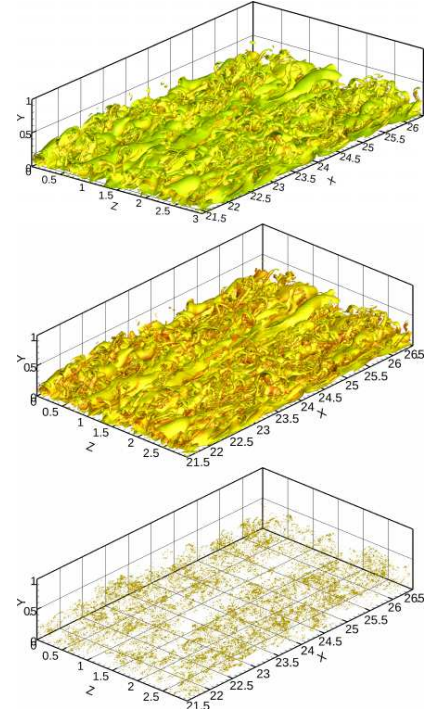


FIG. 4. Total, coherent and incoherent parts of vorticity fields ($|\omega|$) for the transition region $x \in 16.5 - 21.4$ are presented. Iso-values for total and coherent parts are: $|\omega|_{coh} = 5.0$, for incoherent part $|\omega|_{inc} = 0.5$.

more skewed than the PDF of ω_x and ω_y . This behavior is associated with the dominant (streamwise) flow direction and is similar to the transitional and turbulent regions.

Figure 10 shows the PDFs of the incoherent vorticity at different distances away from the wall. The PDFs nearly coincide, thus indicating the homogeneity of the incoherent part of vorticity magnitude.

IV. CORRELATION BETWEEN PRESSURE AND THE INCOHERENT PART VORTICITY

Past research alluded that there may be a possible relationship of the pressure and vorticity components³⁴. However, there is little research into the relationship between pressure fluctuations and incoherent vorticity. For an incompressible channel flow, Kim³⁴ showed a similarity between the spanwise pressure gradient and the streamwise vorticity at the wall. However, he found that the same similarity did not occur for the streamwise pressure gradient and spanwise vorticity. It was (and still is) unclear what causes this behaviour.

This is the author's peer reviewed, accepted manuscript. However, the online version of record will be different from this version once it has been copyedited and typeset.

PLEASE CITE THIS ARTICLE AS DOI: 10.1063/5.0088479

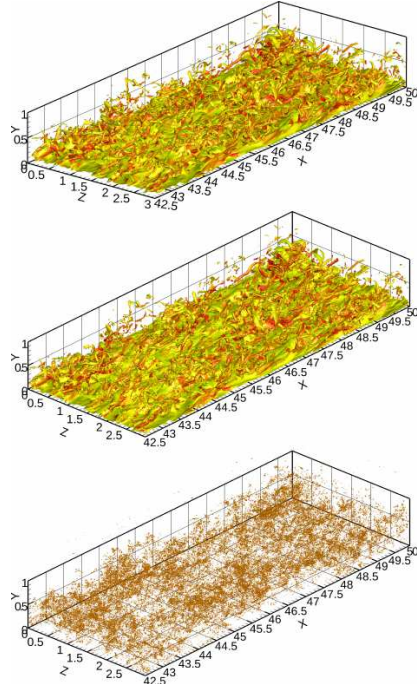


FIG. 5. Total, coherent and incoherent fields of vorticity magnitude for the turbulent region $x \in 42.6 - 50$. Isovalues for total and coherent parts are: $|\omega|_{coh} = 5.0$, for incoherent part $|\omega|_{inc} = 1.2$.

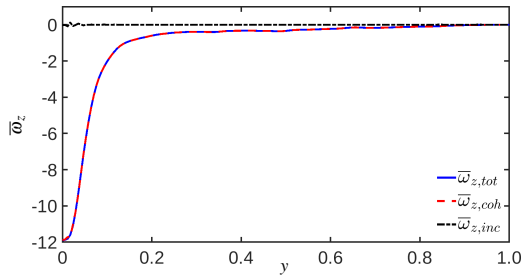


FIG. 6. Spanwise mean vorticity, $\bar{\omega}_z$, for total, coherent and incoherent parts of the flow field.

The wavelet analysis showed that the incoherent part of the vorticity contains a minimal amount of energy compared to the coherent domain. Moreover, it seems to be structureless. We know from Lighthill³⁵ that the instantaneous pressure gradient is related to the vorticity flux $\partial p / \partial x = \partial \omega_z / \partial y$ and $\partial p / \partial z = \partial \omega_x / \partial y$. Because the streamwise and spanwise

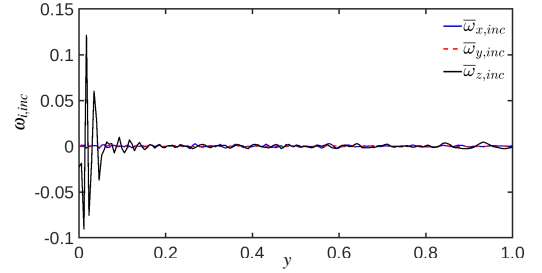


FIG. 7. Incoherent parts of vorticity components averaged in spanwise and streamwise directions in the turbulent region.

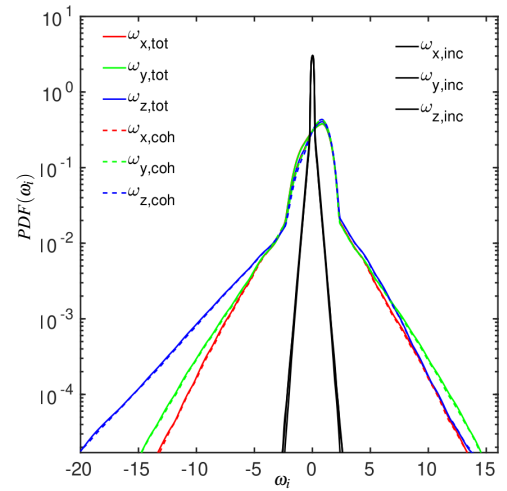


FIG. 8. PDFs of coherent and incoherent parts of vorticity fields for the transition region [21.4 – 26.3], red, green and blue lines, correspondingly.

vorticity components are convected (and diffused) from the wall region, we expect that their incoherent part, regardless of how small energy carries, will interact with the near-wall low-velocity turbulence structures that are associated with the near-wall pressure gradients. In the same vein, we speculate that there might be a correlation between pressure fluctuations and incoherent vorticity. Therefore, we present below an investigation. We have averaged the pressure and incoherent vorticity signals in the spanwise direction. For example, we show the results for $y = 0.02$, $y^+ = 3.6$ in figures 11 and 12. We covered part of the transitional and the entire turbulent region for the wall-pressure and incoherent vorticity magnitude. Furthermore, we show the denoised incoherent part of the vorticity magnitude using the MATLAB wavelet tool³⁶.

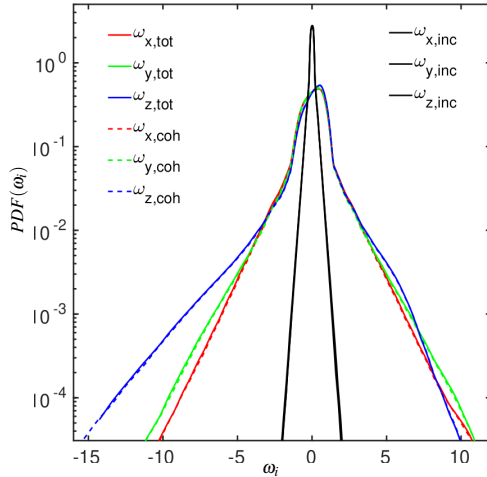


FIG. 9. PDFs of total, coherent and incoherent parts of vorticity components in turbulent region, red, green and blue lines, correspondingly. The PDFs of total and coherent parts are collapsed.

Although there is no one-to-one correspondence between pressure fluctuations and incoherent vorticity, the signal distributions show that some peaks occur in the same (or very similar) positions and a downward slope of signal values in approximately equivalent streamwise segments. For example, increases and peak value positions occur around $x \approx 37, 38.5, 45, 46.5, 48.5$ in the turbulent region for both P and $|\omega|_i$. The downward slope of the signal is also similar in the transition region $x \approx 21$ to 26 . Therefore, to examine further a potential correlation between the wall pressure fluctuation signal and the incoherent vorticity magnitude, we calculated the coefficient R , defined below, at different wall distances; we used the MATLAB function *corrcoef*³⁶:

$$R(P; |\omega|) = \frac{1}{N-1} \sum_{i=1}^N \left(\frac{P_i - \mu_P}{\sigma_P} \right) \left(\frac{|\omega|_i - \mu_{|\omega|}}{\sigma_{|\omega|}} \right), \quad (1)$$

where μ_P , σ_P and $\mu_{|\omega|}$, $\sigma_{|\omega|}$ are mean and standard deviations of pressure fluctuations and incoherent vorticity magnitude. The results for R in the transition and turbulent regions 1 to 6 and at different positions from the wall are given in Table II.

The highest correlation between the wall-pressure fluctuations and the vorticity magnitude is found in the transition region $x \in [21.5 - 26.5]$. The correlation coefficient in this region is $R = 0.58$ at $y^+ = 3.96$ distance from the wall. However, we see a correlation above 26% in all areas for $y^+ \approx 4$. What do the above results mean? Our idea was highly speculative regarding a potential correlation of P and $|\omega|_{inc}$. Although the results are not conclusive about the exact nature of this relationship, they show some correlation. The correlation indicates that the incoherent vorticity part carries physics

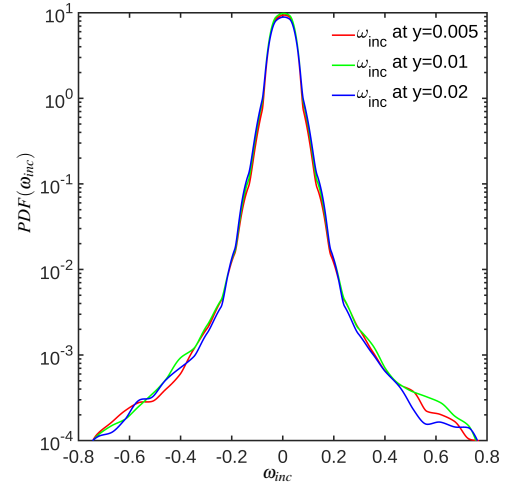


FIG. 10. PDFs of incoherent part of vorticity in turbulent region for the slices at different distance from the wall. The red, green and blue lines correspond to $y = 0.005, 0.01, 0.02$. These values correspond to a range of $y^+ = 1.89 - 3.77$.

	y	y_{max}^+	R
1	0.01	1.42	0.35
	0.02	2.84	0.48
2	0.01	1.76	-0.005
	0.02	3.53	0.15
3	0.01	2.01	0.41
	0.02	4.01	0.58
4	0.01	2.03	0.12
	0.02	4.06	0.38
5	0.01	1.98	0.10
	0.02	4.06	0.35
6	0.005	1.90	0.2
	0.02	3.77	0.26

TABLE II. Correlation coefficient for P and $|\omega|_{inc}$ in different transitional and turbulent regions. The reported y^+ value is the maximum value calculated in each region.

properties related to pressure fluctuation and, hence, to near-wall acoustics. Furthermore, we speculate that the thermodynamic properties of the wall would affect this relationship. Finally, we allude that if a further investigation proves the above true, we could recover from the velocity field, the incoherent vorticity, and the sound properties of the field. The above are topics of our current and future research.

V. CONCLUSIONS

DNS data of turbulent compressible boundary layer flow were analyzed using the CVE method. The flow has been de-

This is the author's peer reviewed, accepted manuscript. However, the online version of record will be different from this version once it has been copyedited and typeset.

PLEASE CITE THIS ARTICLE AS DOI: 10.1063/1.50088479

7

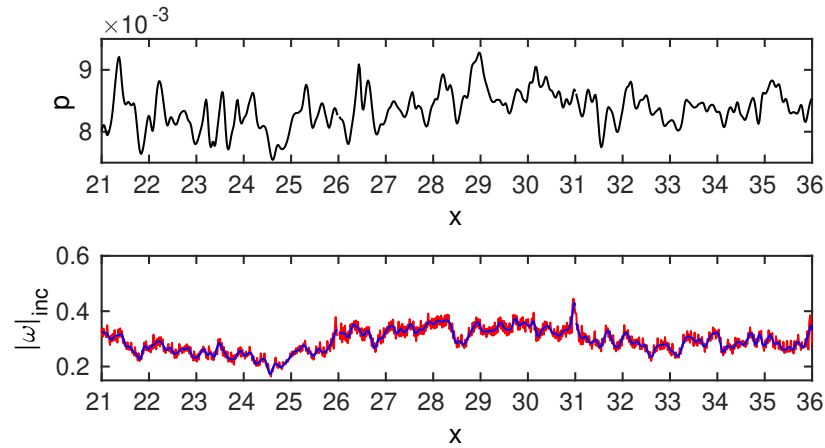


FIG. 11. Transitional region: Pressure fluctuation (p) and incoherent vorticity magnitude ($|\omega|_{inc}$) averaged in the spanwise direction. For the incoherent vorticity magnitude, we present the actual signal (red line) and the denoised signal (blue line). The results correspond to the boundary layer position $y = 0.02$.

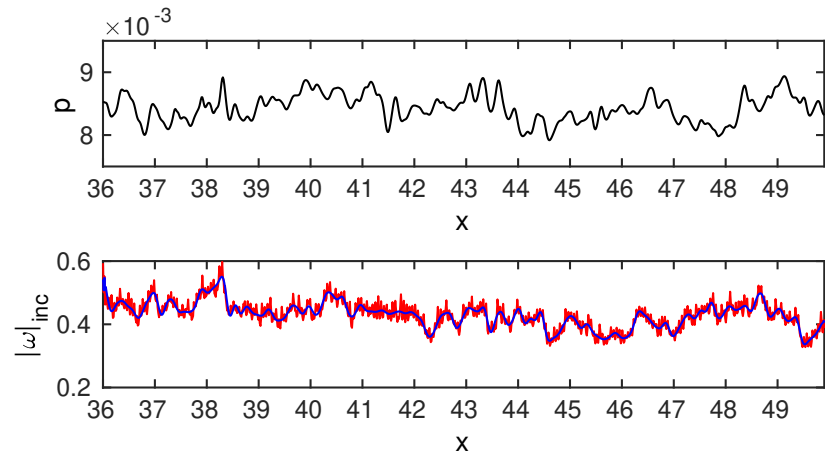


FIG. 12. Turbulent region: Pressure fluctuation (p) and incoherent vorticity magnitude ($|\omega|_{inc}$) averaged in the spanwise direction. For the incoherent vorticity magnitude, we present the actual signal (red line) and the denoised signal (blue line). The results correspond to the boundary layer position $y = 0.02$.

composed into coherent and incoherent parts by thresholding the wavelet coefficients with one scale in three spatial directions. We found that few wavelet coefficients are sufficient to represent the flow's coherent structures. Furthermore, the coherent component carries most of the energy. The PDFs of the vorticity components are skewed for the coherent part (and total). Instead, the PDFs of the incoherent components are symmetric for all vorticity components in both the transition and turbulent region.

The incoherent part of vorticity appears to be without an apparent topological structure and low amplitude. However, further analysis shows a correlation between the pressure fluctuations and the incoherent vorticity. The highest correlation is found in the transition region at $y^+ \approx 4$. Although further studies are required to understand the nature of the incoherent part, it appears that there is some correlation with the wall pressure fluctuations. We aim to shed light on the above issue by further analyzing shock/boundary-layer interaction data to

examine if the above behavior is consistent in other types of flow.

VI. ACKNOWLEDGMENTS

This material is based upon work supported by the Air Force Office of Scientific Research under award number FA9550-19-1-7018. The U.S. Government is authorized to reproduce and distribute reprints for Governmental purpose notwithstanding any copyright notation thereon. The authors would like to thank Dr. Garner for his support.

GK acknowledges M. Farge and K. Schneider for their insightful discussions regarding the wavelet theory over the years.

VII. AUTHOR DECLARATIONS

The authors have no conflicts to disclose.

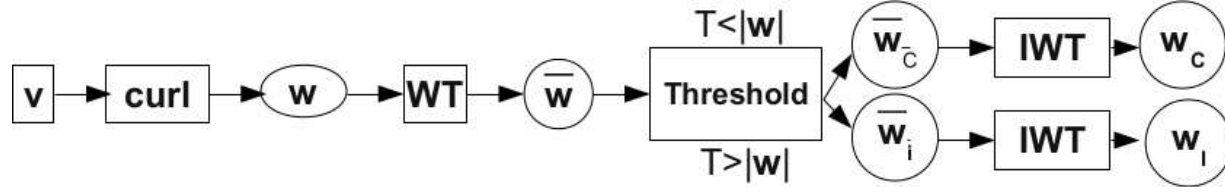
VIII. DATA AVAILABILITY

The data that support the findings of this study are available from the corresponding author upon reasonable request.

- ¹C.-H. Zhang, Q. Tang, and C.-B. Lee, "Hypersonic boundary-layer transition on a flared cone," *Acta Mech. Sin.* **29**, 48–53 (2013).
- ²K. M. Casper, S. J. Beresh, and S. P. Schneider, "Pressure fluctuations beneath instability wavepackets and turbulent spots in a hypersonic boundary layer," *J. Fluid Mech.* **756**, 1058–1091 (2014).
- ³Y. Zhu, C. Zhang, X. Chen, H. Yuan, J. Wu, S. Chen, and C. Lee, "Transition in hypersonic boundary layers: Role of dilatational waves," *AIAA Journal* **54**, 3039–3049 (2016).
- ⁴K. M. Casper, S. J. Beresh, J. F. Henfling, R. W. Spillers, and B. O. M. Pruett, "Hypersonic wind-tunnel measurements of boundary-layer transition on a slender cone," *AIAA Journal* **54**, 1250–1263 (2016).
- ⁵L. Duan, I. Beekman, and M. P. Martín, "Direct numerical simulation of hypersonic turbulent boundary layers. part 3. effect of mach number," *J. Fluid Mech.* **672**, 245–267 (2011).
- ⁶K. J. Franko and S. K. Lele, "Breakdown mechanisms and heat transfer overshoot in hypersonic zero pressure gradient boundary layers," *J. Fluid Mech.* **730**, 491–532 (2013).
- ⁷J. Sivasubramanian and H. F. Fasel, "Direct numerical simulation of transition in a sharp cone boundary layer at mach 6: fundamental breakdown," *J. Fluid Mech.* **768**, 175–218 (2015).
- ⁸K. Ritos, D. Drikakis, I. W. Kokkinakis, and S. M. Spottswood, "Computational aeroacoustics beneath high speed transitional and turbulent boundary layers," *Computers and Fluids* **203**, 104520 (2020).
- ⁹K. Ritos, D. Drikakis, and I. Kokkinakis, "Acoustic loading beneath hypersonic transitional and turbulent boundary layers," *Journal of Sound and Vibration* **441**, 50 – 62 (2019).
- ¹⁰L. Duan, M. M. Choudhari, and C. Zhang, "Pressure fluctuations induced by a hypersonic turbulent boundary layer," *Journal of Fluid Mechanics* **804**, 578–607 (2016).
- ¹¹X. Zhao and L. Zhao, "Wall pressure fluctuations beneath hypersonic boundary layer over plate," *AIAA Journal* , 1–10 (2020).
- ¹²J. Huang, L. Duan, K. Casper, R. Wagnild, and N. Bitter, "Direct numerical simulation of turbulent pressure fluctuations over a cone at Mach 8," in *AIAA SciTech Forum*, AIAA 2020-1065 (2020).
- ¹³D. Drikakis, K. Ritos, S. M. Spottswood, and Z. B. Riley, "Flow transition to turbulence and induced acoustics at mach 6," *Physics of Fluids* **33**, 076112 (2021).
- ¹⁴K. Schneider and O. Vasilyev, *Annu. Rev. Fluid Mech.* **42**, 473 (2010).
- ¹⁵M. Farge, *Annu. Rev. Fluid Mech.* **24**, 395 (1992).
- ¹⁶M. Farge, K. Schneider, and N. Kevlahan, *Phys. Fluids* **11**, 2187 (1999).
- ¹⁷M. Farge, G. Pellegrino, and K. Schneider, *Phys. Rev. Lett.* **87**, 45011 (2001).
- ¹⁸K. Schneider, M. Farge, G. Pellegrino, and M. Rogers, *J. Fluid Mech.* **534**, 39 (2005).
- ¹⁹N. Okamoto, K. Yoshimatsu, K. Schneider, M. Farge, and Y. Kaneda, *Phys. Fluids* **19**, 1 (2007).
- ²⁰G. Khujadze, R. Nguyen van yen, K. Schneider, M. Oberlack, and M. Farge, "Coherent vorticity extraction in turbulent boundary layers using orthogonal wavelets," in *Center for Turbulence Research, Center for Turbulence Research Proceedings of the Summer Program 2010* (Stanford University and NASA-Ames, 2010).
- ²¹T. Sakurai, K. Yoshimatsu, K. Schneider, M. Farge, K. Morishita, and T. Ishihara, "Coherent structure extraction in turbulent channel flow using boundary adapted wavelets," *Journal of Turbulence* **18**(4), 352–372 (2017).
- ²²I. Kokkinakis, D. Drikakis, K. Ritos, and S. M. Spottswood, "Direct numerical simulation of supersonic flow and acoustics over a compression ramp," *Physics of Fluids* **32**, 066107 (2020).
- ²³R. E. Spall and M. R. Malik, "Goertler vortices in supersonic and hypersonic boundary layers," *Physics of Fluids A: Fluid Dynamics* **1**, 1822–1835 (1989).
- ²⁴N. M. El-Hady, "Nonparallel instability of supersonic and hypersonic boundary layers," *Physics of Fluids A: Fluid Dynamics* **3**, 2164–2178 (1991).
- ²⁵M. Lagha, J. Kim, J. D. Eldredge, and X. Zhong, "A numerical study of compressible turbulent boundary layers," *Physics of Fluids* **23**, 015106 (2011).
- ²⁶Y. Zhu, X. Chen, J. Wu, S. Chen, C. Lee, and M. Gad-el Hak, "Aerodynamic heating in transitional hypersonic boundary layers: Role of second-mode instability," *Physics of Fluids* **30**, 011701 (2018).
- ²⁷J. Liu, J. Xu, C. Wang, P. Yu, and J. Bai, "Pressure gradient effects on the secondary instability of mack mode disturbances in hypersonic boundary layers," *Physics of Fluids* **33**, 014109 (2021).
- ²⁸M. Morkovin, "Effects of compressibility on turbulent flows," in *The Oxford Handbook of Innovation*, edited by A. Favre (Gordon and Breach, New York, 1962) pp. 367–380.
- ²⁹P. Bradshaw, "Compressible turbulent shear layers," *Annual review of Fluid Mechanics* **9**, 33–54 (1977).
- ³⁰V. S. K. W. Shyy, "Compressibility effects in modeling complex turbulent flows," *Prog. Aerospace Sci.* **33**, 587–645 (1997).
- ³¹S. Mallat, *A wavelet tour of signal processing* (Academic Press, 2010).
- ³²I. Daubechies, *Ten Lectures on wavelets* (SIAM, Philadelphia, 1992).
- ³³D. Donoho, "Unconditional bases are optimal bases for data compression and statistical estimation," *Appl. Comput. Harmon. Anal.* **1**, 100–115 (1993).
- ³⁴J. Kim, "On the structure of pressure fluctuations in simulated turbulent channel flow," *Journal of Fluid Mechanics* **205**, 421–451 (1989).
- ³⁵M. Lighthill, *Boundary layer theory, in Laminar boundary layers* (Oxford University Press, 1963).
- ³⁶MATLAB Wavelet Toolbox, "Matlab wavelet toolbox," (2018), the Math-Works, Natick, MA, USA.

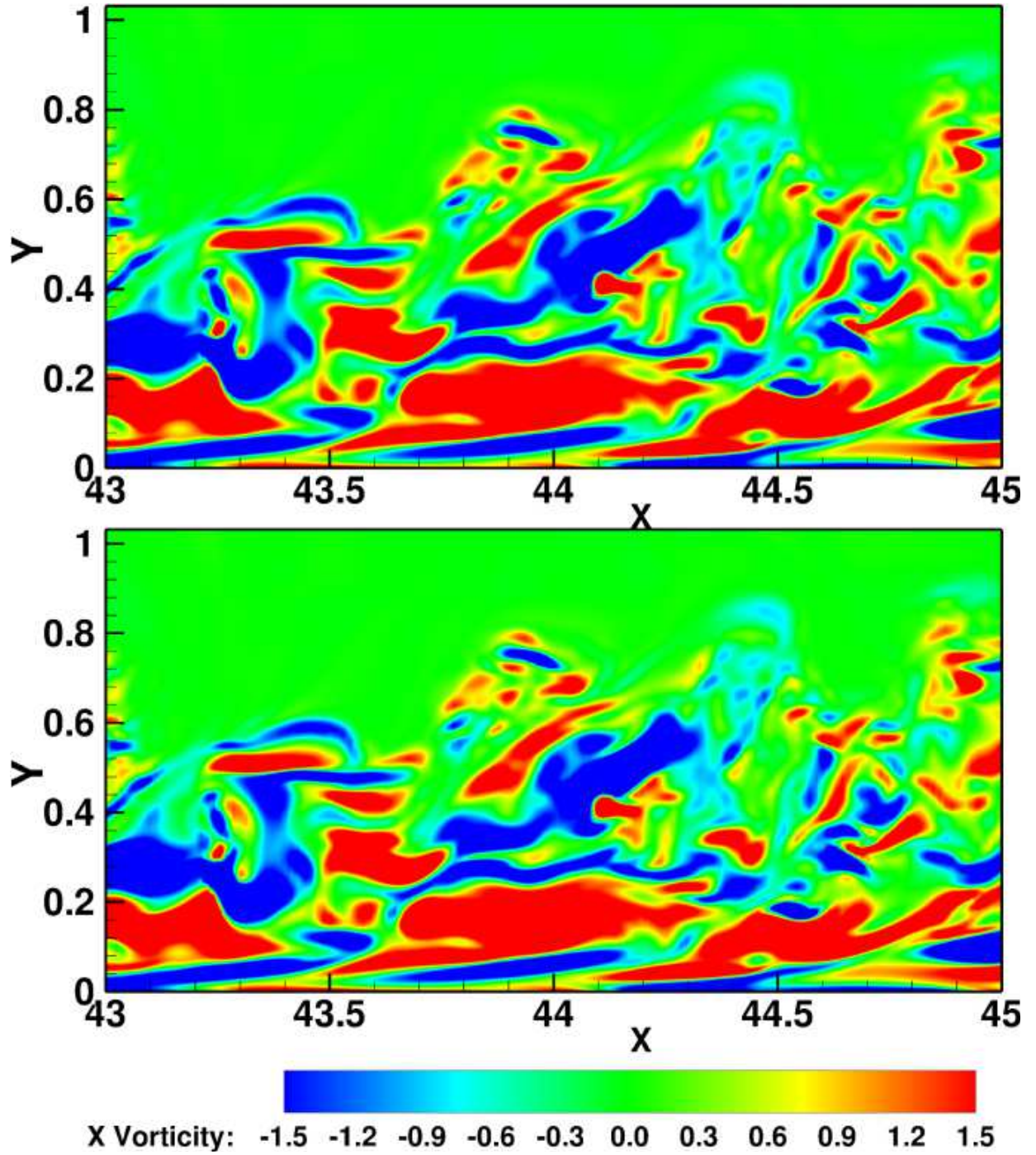
This is the author's peer reviewed, accepted manuscript. However, the online version of record will be different from this version once it has been copyedited and typeset.

PLEASE CITE THIS ARTICLE AS DOI: 10.1063/5.0088479



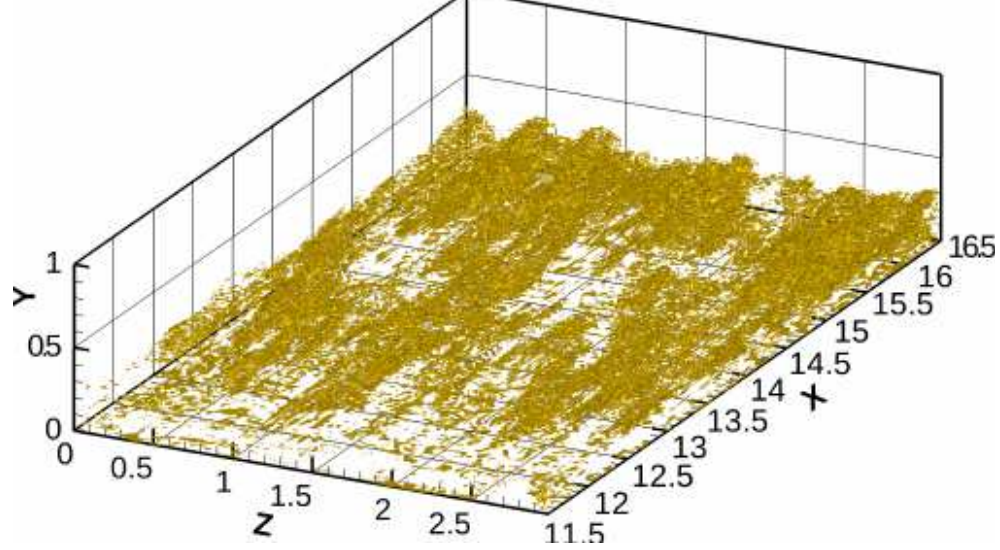
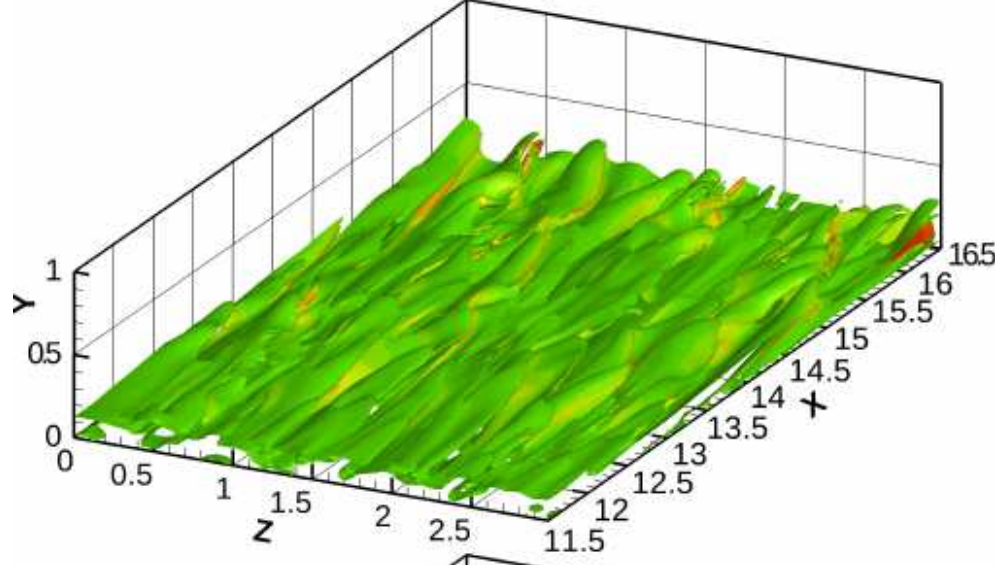
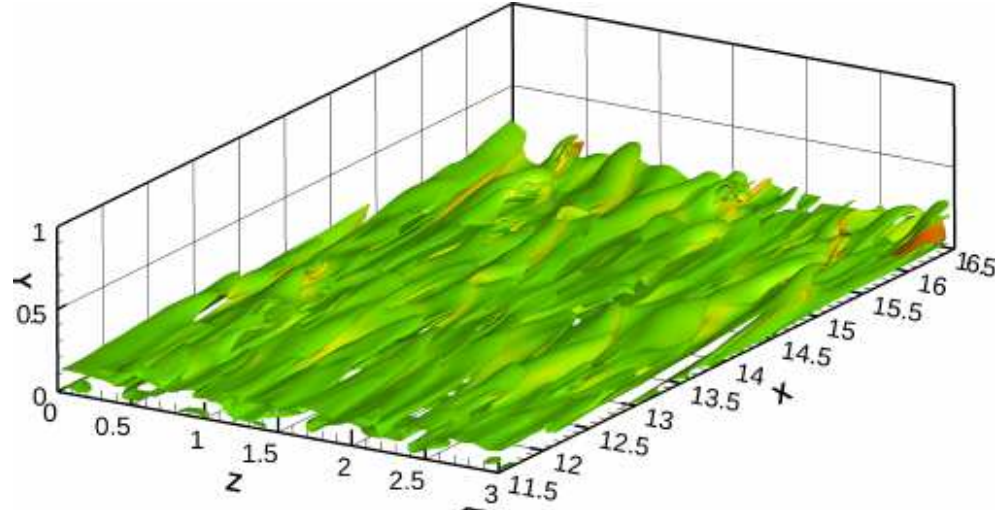
This is the author's peer reviewed, accepted manuscript. However, the online version of record will be different from this version once it has been copyedited and typeset.

PLEASE CITE THIS ARTICLE AS DOI: 10.1063/5.0088479



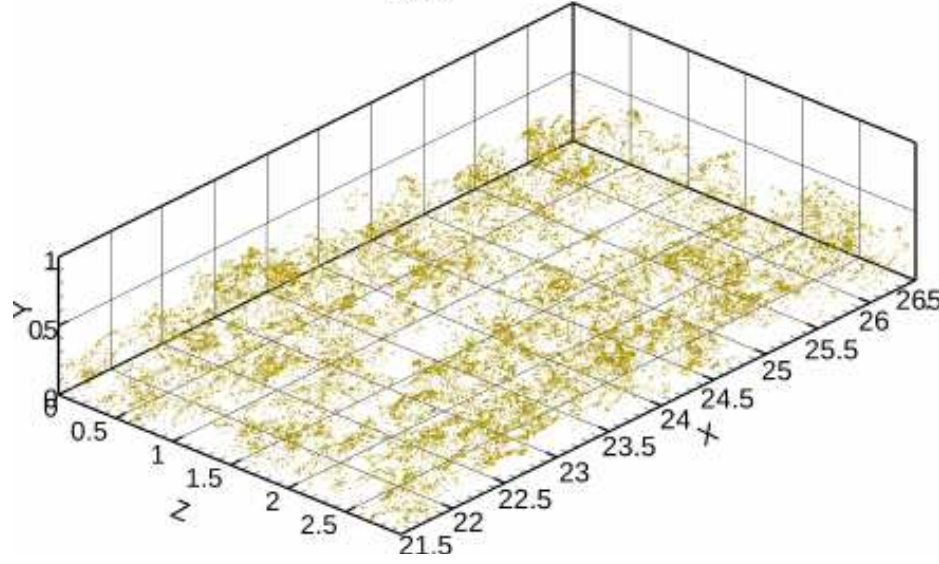
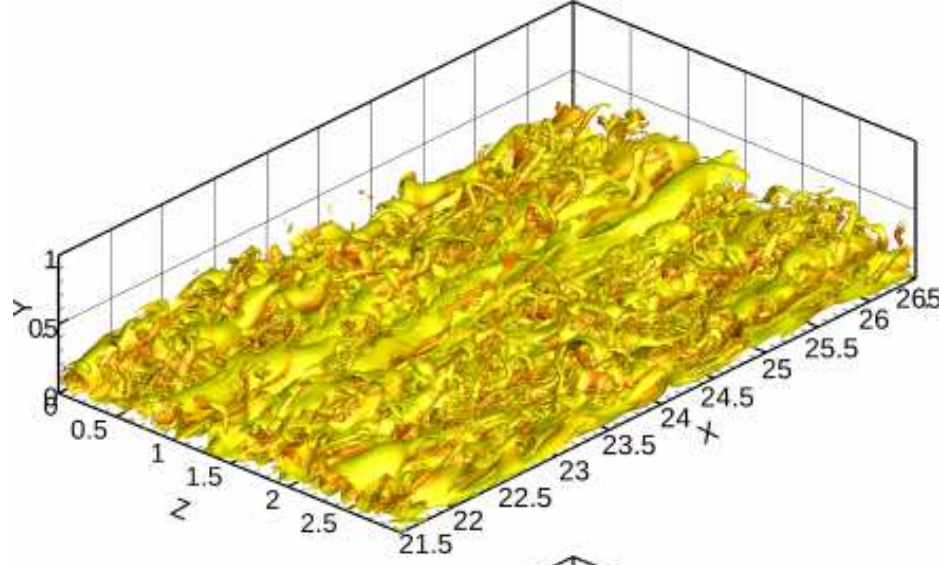
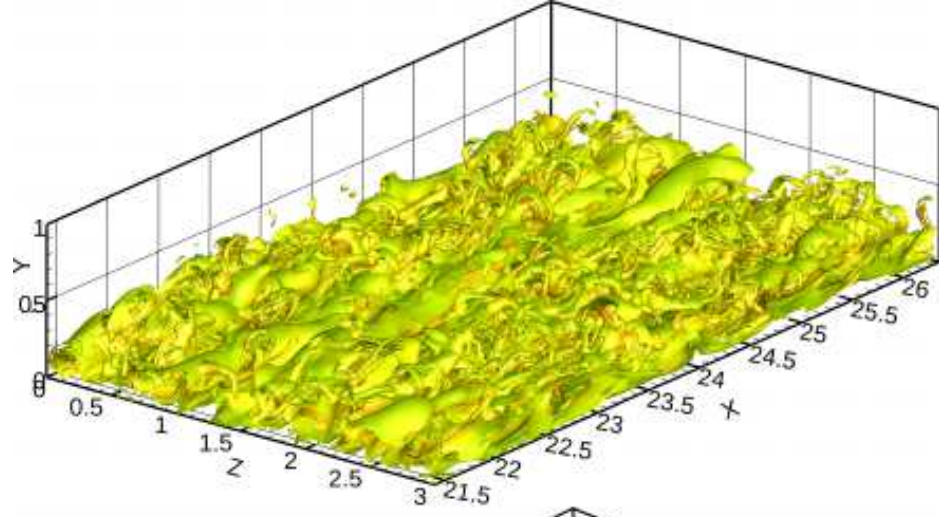
This is the author's peer reviewed, accepted manuscript. However, the online version of record will be different from this version once it has been copyedited and typeset.

PLEASE CITE THIS ARTICLE AS DOI: 10.1063/5.0088479



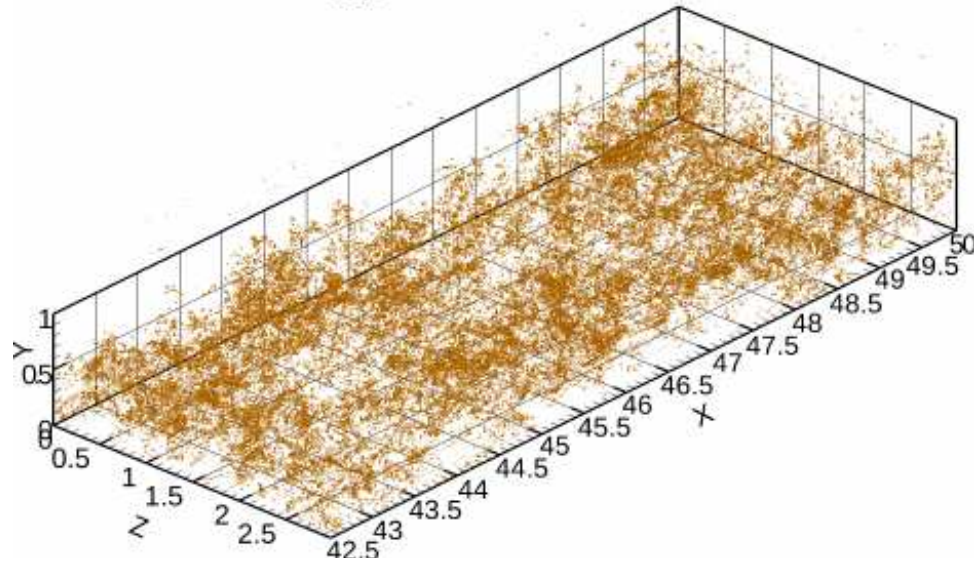
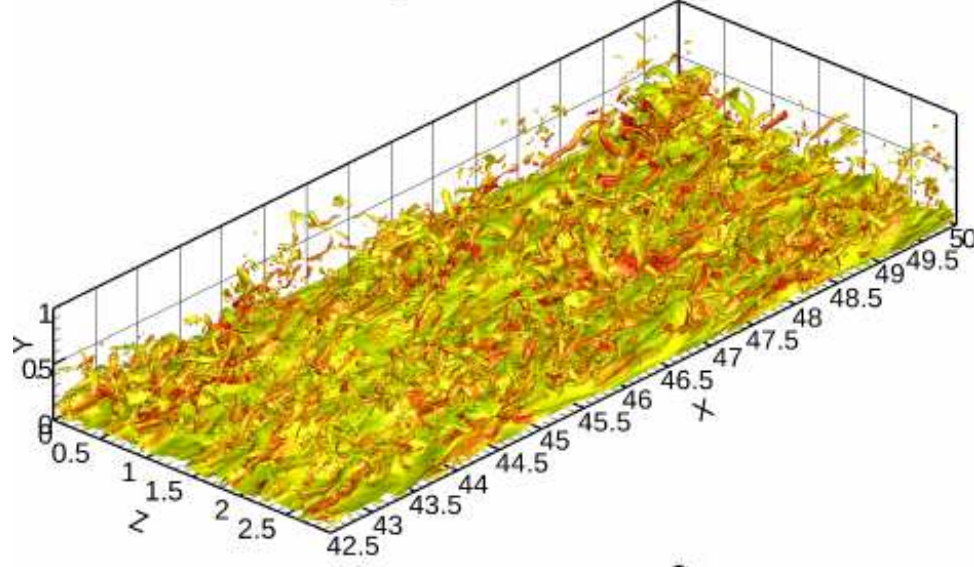
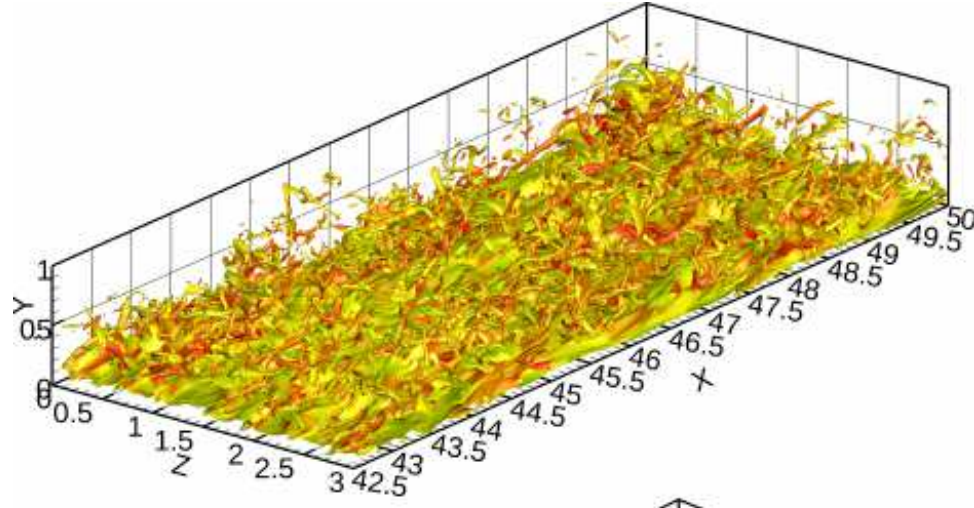
This is the author's peer reviewed, accepted manuscript. However, the online version of record will be different from this version once it has been copyedited and typeset.

PLEASE CITE THIS ARTICLE AS DOI: 10.1063/1.50088479



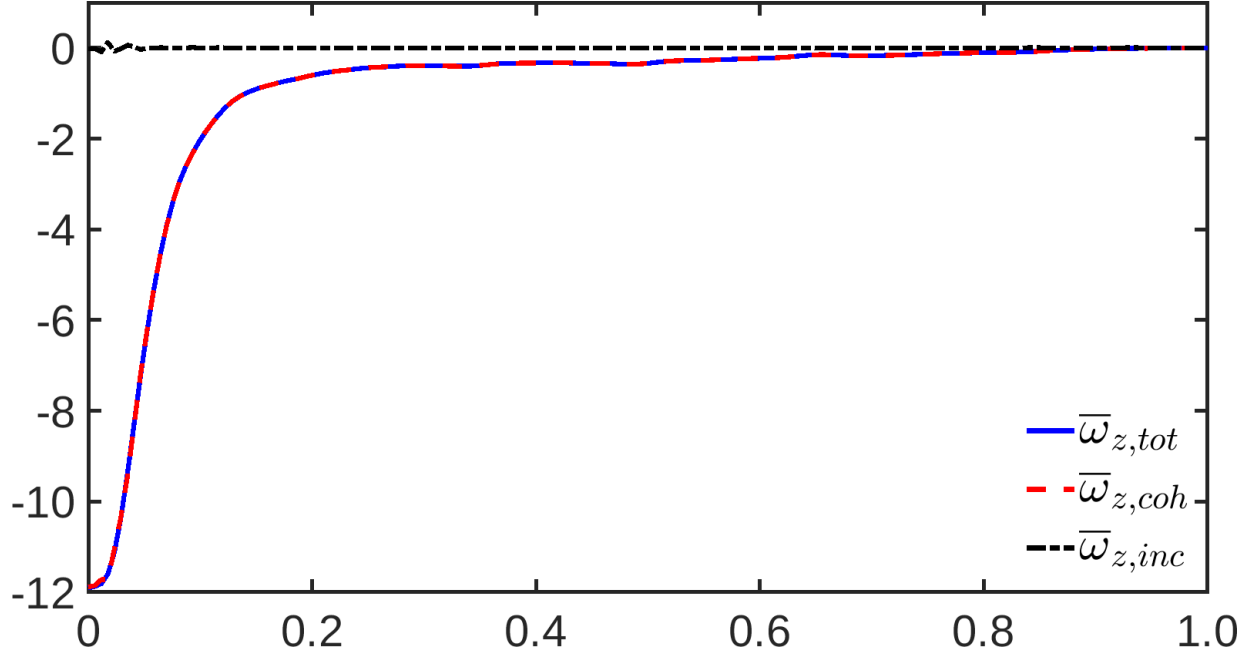
This is the author's peer reviewed, accepted manuscript. However, the online version of record will be different from this version once it has been copyedited and typeset.

PLEASE CITE THIS ARTICLE AS DOI: 10.1063/5.0088479



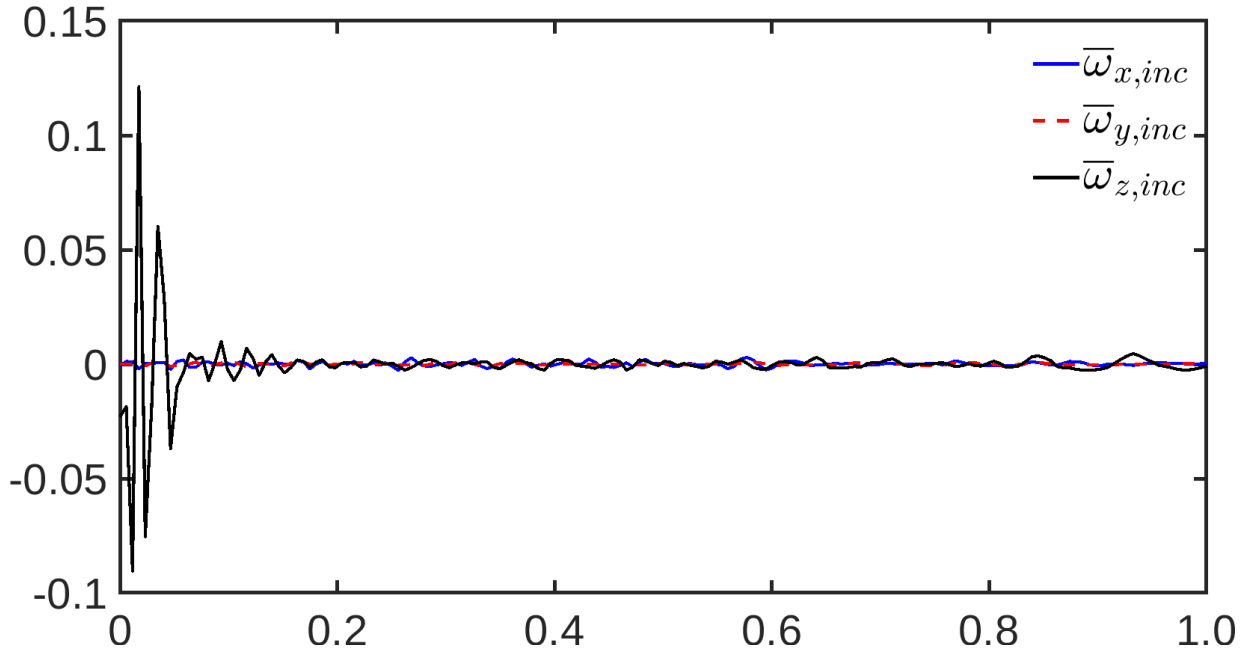
This is the author's peer reviewed, accepted manuscript. However, the online version of record will be different from this version once it has been copyedited and typeset.

PLEASE CITE THIS ARTICLE AS DOI: 10.1063/1.50088479



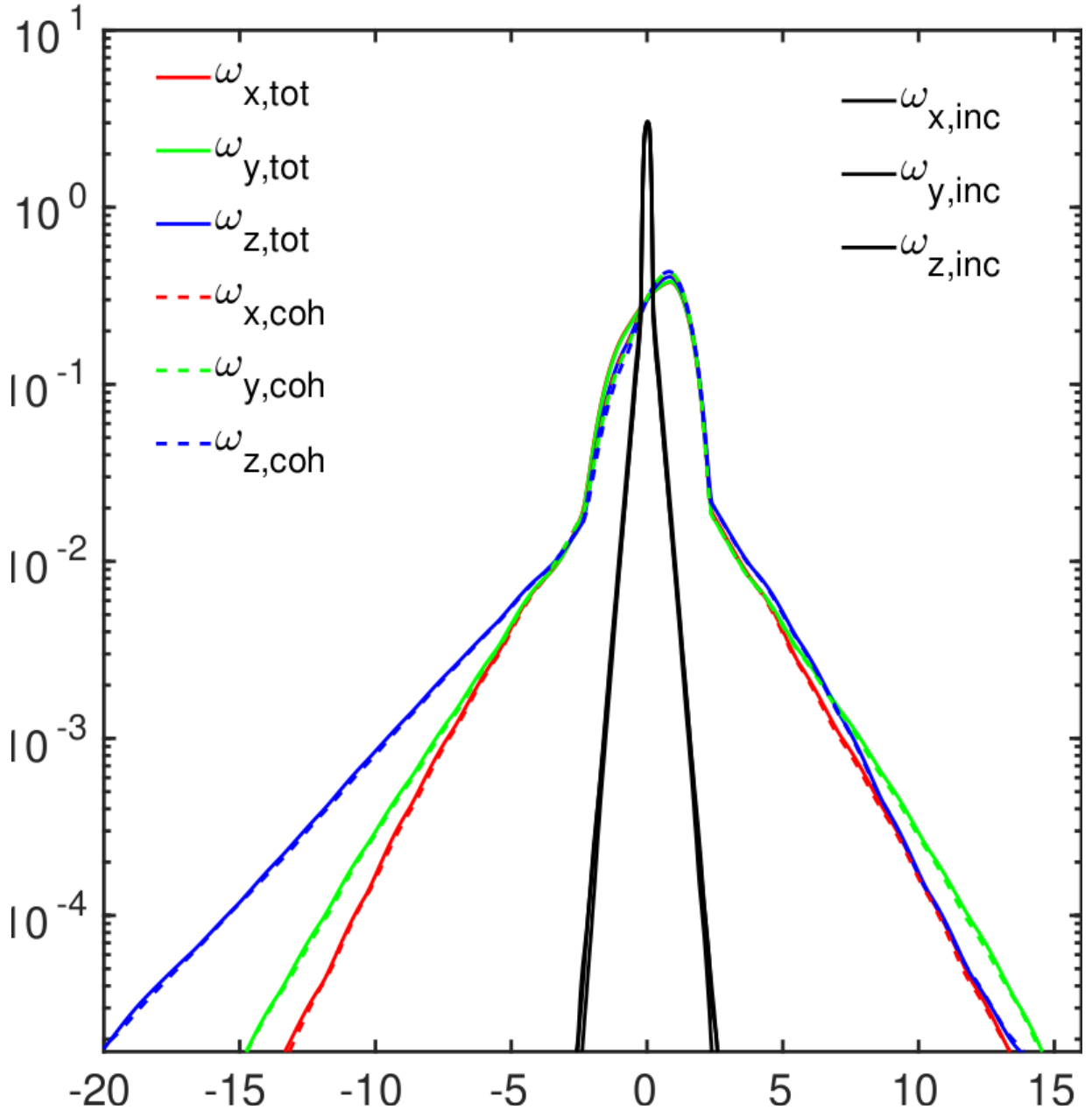
This is the author's peer reviewed, accepted manuscript. However, the online version of record will be different from this version once it has been copyedited and typeset.

PLEASE CITE THIS ARTICLE AS DOI: 10.1063/1.50088479



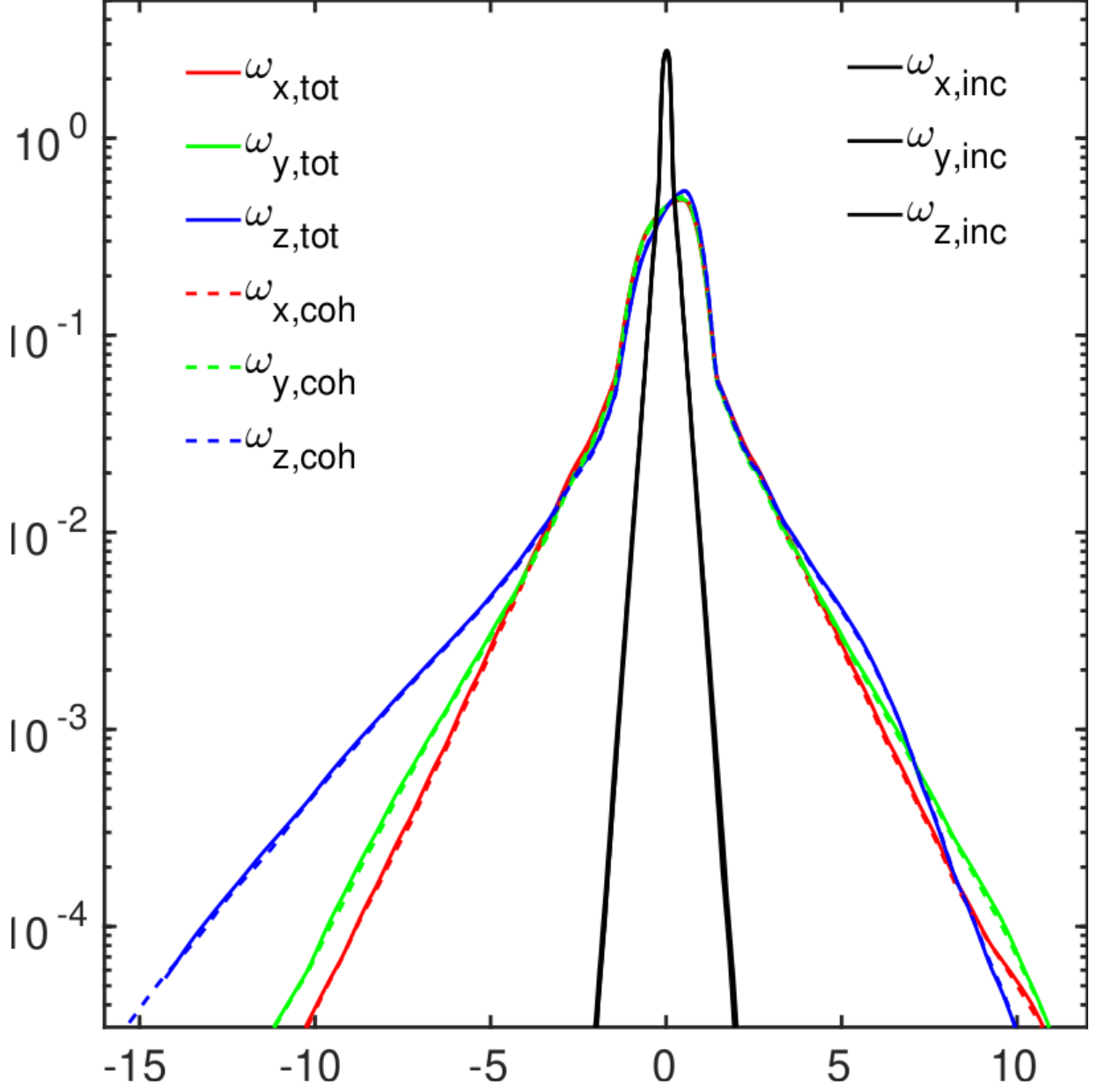
This is the author's peer reviewed, accepted manuscript. However, the online version of record will be different from this version once it has been copyedited and typeset.

PLEASE CITE THIS ARTICLE AS DOI: 10.1063/5.0088479



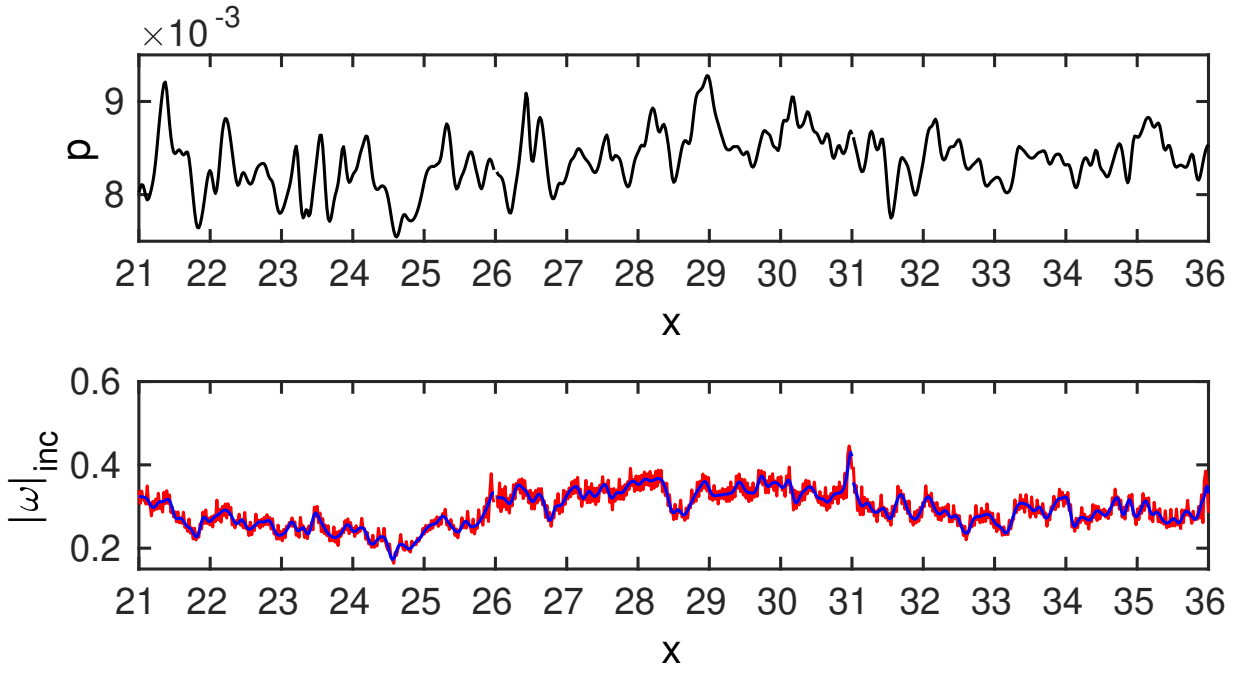
This is the author's peer reviewed, accepted manuscript. However, the online version of record will be different from this version once it has been copyedited and typeset.

PLEASE CITE THIS ARTICLE AS DOI: 10.1063/5.0088479



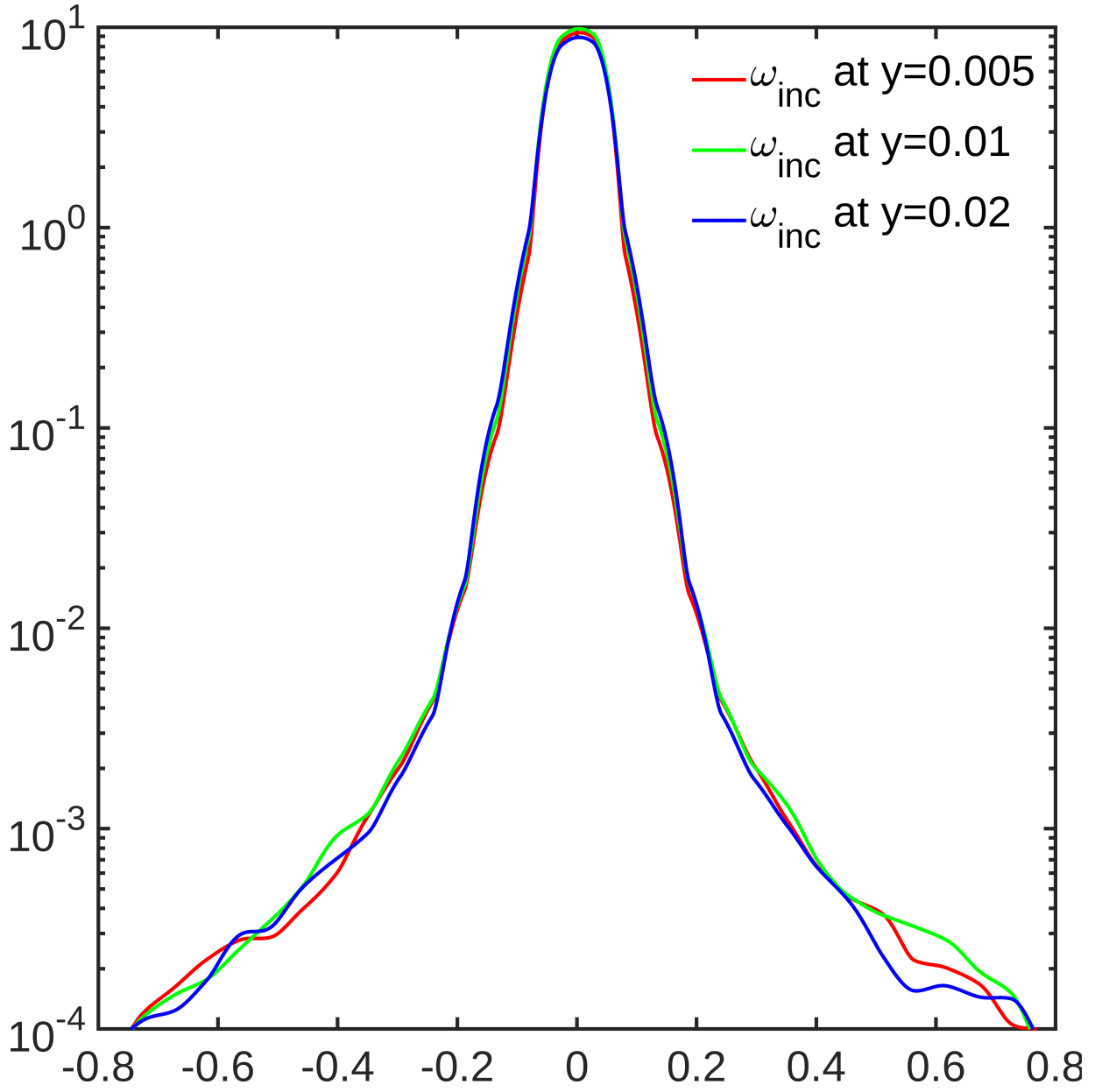
This is the author's peer reviewed, accepted manuscript. However, the online version of record will be different from this version once it has been copyedited and typeset.

PLEASE CITE THIS ARTICLE AS DOI: 10.1063/1.50088479



This is the author's peer reviewed, accepted manuscript. However, the online version of record will be different from this version once it has been copyedited and typeset.

PLEASE CITE THIS ARTICLE AS DOI: 10.1063/1.50088479



This is the author's peer reviewed, accepted manuscript. However, the online version of record will be different from this version once it has been copyedited and typeset.

PLEASE CITE THIS ARTICLE AS DOI: 10.1063/1.50088479

